Effects of GaN channel downscaling in AlGaN–GaN high electron mobility transistor structures grown on AlN bulk substrate

Reda Elwaradi, Jash Mehta, Thi Huong Ngo, Maud Nemoz, Catherine Bougerol, Farid Medjdoub, Yvon Cordier

Journal of Applied Physics

RESEARCH ARTICLE | APRIL 13 2023

Effects of GaN channel downscaling in AlGaN–GaN high electron mobility transistor structures grown on AlN bulk substrate

Reda Elwaradi; Jash Mehta; Thi Huong Ngo; ... et. al

Journal of Applied Physics 133, 145705 (2023)
https://doi.org/10.1063/5.0147048

AIP Publishing

Journal of Applied Physics ARTICLE scitation.org/journal/jap

Effects of GaN channel downscaling in AlGaN–GaN high electron mobility transistor structures grown on AlN bulk substrate

Cite as: J. Appl. Phys. **133**, 145705 (2023); doi: 10.1063/5.0147048
Submitted: 18 February 2023 · Accepted: 30 March 2023 ·
Published Online: 13 April 2023

Reda Elwaradi,[1,2] Jash Mehta,[3] Thi Huong Ngo,[1] Maud Nemoz,[1] Catherine Bougerol,[4] Farid Medjdoub,[3] and Yvon Cordier[1,a)]

AFFILIATIONS

[1]Université Côte d'Azur, CNRS, CRHEA, rue B. Grégory, 06560 Valbonne, France
[2]STMicroelectronics SA, 850 rue Jean Monet, Bâtiment 6000, 38920 Crolles, France
[3]IEMN, CNRS, University of Lille, 59650 Villeneuve d'Ascq, France
[4]Univ. Grenoble Alpes, CNRS, Grenoble INP, Institut Néel, 38000 Grenoble, France

[a)]**Author to whom correspondence should be addressed:** yc@crhea.cnrs.fr

ABSTRACT

In this work, two series of AlGaN/GaN/AlN high electron mobility transistor (HEMT) heterostructures have been grown by molecular beam epitaxy on AlN bulk substrates. The effects of reduction in the GaN channel thickness as well as the AlGaN barrier thickness and composition on structural and electrical properties of the heterostructures have been studied. The material analysis involved high-resolution x-ray diffraction, atomic force microscopy, and cross-sectional transmission electron microscopy. In a first series of HEMT structures grown with an aluminum content of 30% in the AlGaN barrier, the channel downscaling results in a reduction in the GaN strain relaxation rate but at the expense of degradation in the mean crystal quality and in the electron mobility with a noticeable increase in the sheet resistance. An opposite trend is noticed for the three-terminal breakdown voltage of transistors, so that a trade-off is obtained for a 50 nm width GaN channel HEMT, which exhibits a sheet resistance of 1700 Ω/sq. with transistors demonstrating three-terminal breakdown voltage up to 1400 V for 40 μm gate to drain spacing with static on resistance $R_{on} = 32\ m\Omega\ cm^2$. On the other hand, a second series of HEMT structures with high aluminum content AlGaN barriers and sub-10 nm GaN channels have been grown perfectly strained with high sheet carrier densities allowing to preserve sheet resistances in the range of 880–1050 Ω/sq.

INTRODUCTION

AlGaN/GaN high electron mobility transistors (HEMTs) are widely studied for high-power and high-frequency applications thanks to their remarkable material and device characteristics. The formation of a high mobility two-dimensional electron gas (2DEG) in the GaN channel at the interface with the larger energy bandgap AlGaN barrier is the key of the success of these devices.[1] To push further the limits for high voltage applications (>1200 V), the use of ultra-wide bandgap (UWBG) materials such as AlN is now under investigation due to their intrinsic properties.[2–4] Indeed, AlN presents a higher critical electric field and thermal conductivity[5] than those of the GaN material, and as a buffer layer, it enables to sustain extremely high voltages.[6–8] Furthermore, due to the difference in polarization charges with the channel material, AlN, as a buffer layer, can behave as a back-barrier to improve the confinement of carriers located in the 2DEG. Last, the replacement of GaN by AlGaN as the channel material is also considered to increase the critical electric field and make transistors with extremely high breakdown voltages.[9–11] However, the achievement of low-resistance ohmic contacts with 2DEGs generated at the interface with high Al-content AlGaN remains a challenge to combine low on-resistance with a high breakdown voltage.[12,13] For this reason, trying to keep a GaN channel in ultimate all binary AlN/GaN/AlN or in Al-rich AlGaN/GaN/AlN heterostructures is an interesting compromise to maintain low on-resistance provided the high breakdown voltage is achieved. In our previous work, we investigated the effect of the GaN channel thickness and the

AlGaN barrier composition of HEMT structures grown on AlN-on-sapphire on the lateral breakdown voltage.[8,14] While a 240 nm thick channel HEMT presented a buffer lateral breakdown voltage (BV) of 270 V for 2 μm spaced contacts, the structure containing an 8 nm GaN channel exhibited a BV of 1 kV, resulting in a critical electric field reaching 5 MV/cm. However, the thin channel structure presented a peculiar surface corrugation[14] so that highly anisotropic transport properties were obtained in the channel. To overcome this drawback and to avoid any effect related to the quality of AlN, we aimed at investigating the effect of the GaN channel thickness in HEMT epilayers grown on bulk AlN substrates. For this purpose, AlGaN/GaN/AlN HEMT structures were grown with GaN channel thickness varying from 500 to 8 nm. The epi-layers' structural quality as well as the properties of the electron gas located in the GaN channel, the lateral buffer breakdown voltage, and the three-terminal breakdown voltage of transistors fabricated with isolated gates were investigated.

EXPERIMENTAL

Different structures were grown by ammonia source molecular beam epitaxy (NH_3-MBE) in a Riber Compact 21 reactor[15] on Al-polar 1-in. and 2-in. diameter commercial bulk AlN substrates from HexaTech Inc. (AlN-10 series) with dislocation density below $10^3/cm^2$.[16] To evaluate the effect of the GaN channel thickness on HEMT structural and electrical properties, a series of HEMT structures have been grown with a thin AlN buffer layer and a GaN channel of thickness varying from 500 down to 8 nm (Fig. 1). The first part of the structures contains a barrier layer consisting of a 1 nm AlN spacer plus a 19 nm AlGaN layer with a nominal Al content of 30% capped with a thin GaN layer. As shown later, the reduction in strain relaxation in the GaN channel while shrinking its thickness led us to change the AlGaN barrier composition to 82%–86% Al content AlGaN for the last samples. In order to better control the growth temperature, the back-side of the AlN substrates was coated with 1 μm thick sputtered molybdenum. An infrared pyrometer operating close to 1 μm wavelength was used after calibrations based on the GaN evaporation rate under vacuum. Reflection high energy electron diffraction (RHEED) patterns were observed during the growth. The substrates were first chemically prepared with a dip into diluted HF, rinsing in de-ionized water, and blowing under nitrogen prior to introduction in the high vacuum preparation chamber where they were heated up to 600 °C according to a thermocouple. After transfer into the growth chamber, the RHEED patterns were not possible to observe until a temperature of about 500 °C was reached due to charging effects attesting the high insulating character of AlN. The substrate was covered several times with gallium until the RHEED streaky

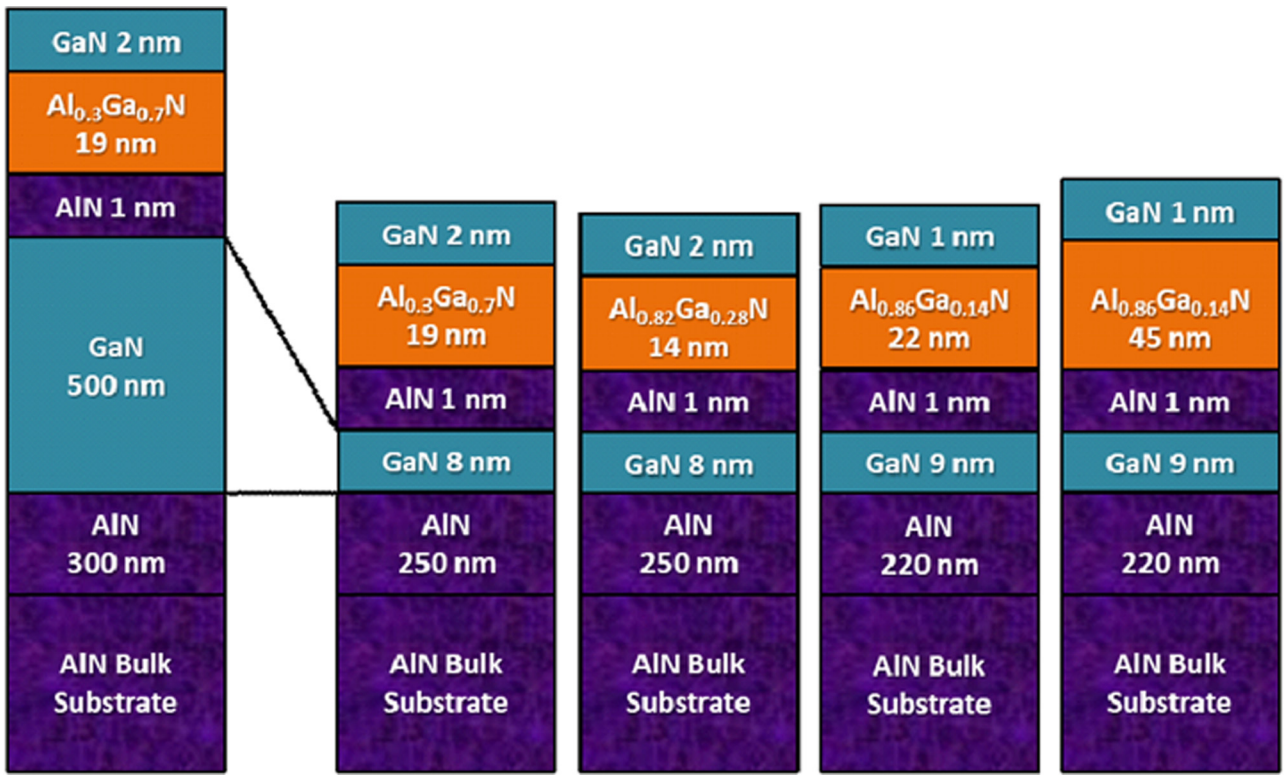

FIG. 1. Cross section of high electron mobility transistor (HEMT) epi-layers grown on the bulk AlN substrate.

pattern disappeared and heated up to about 920 °C to remove residual oxygen contamination from the surface. A constant NH_3 flow rate of 200 SCCM was used for the totality of the process. The growth of AlN buffer layers started at temperatures ranging from 830 to 880 °C and continued between 900 and 920 °C. According to calibrations, the growth rate for AlN was 100 nm/h and the growth occurs under a nitrogen-rich regime. The thickness of the AlN buffer layer in the studied samples is reported in Tables I and II. Prior to the growth of the GaN channel, the growth was stopped for several minutes in order to reach the 780–800 °C range at which GaN and the rest of the HEMT structure is usually grown.[15] Then, a very thin AlN layer (maximum 1 nm) was grown to avoid any roughness development due to the low Al adatom surface mobility before the GaN channel followed by a 1 nm AlN exclusion layer and the AlGaN barrier layer capped with 1–2 nm GaN. The surface morphology was studied by tapping mode atomic force microscopy (AFM). High-resolution x-ray diffraction (XRD) with a Kα1 Cu line was used to assess the crystal quality of the grown layers as well as the strain state of GaN. In particular, the full width at half maximum (FWHM) of omega scan peaks (rocking curves) for symmetric (002) and asymmetric (302) reflections helps to compare the quality of different GaN layers. 2theta-omega scans were performed around (004) reflections, and reciprocal space mapping (RSM) around the (105) reflection was used to attest the absence of strain relaxation in the thinnest GaN channel. In addition, scanning transmission electron microscopy (STEM) experiments were performed on samples prepared in cross sections using a FEI-Tecnai operated at 200 kV. The 2DEG electron density was measured by mercury probe capacitance–voltage (Hg-CV) or by Hall effect, and the sheet resistance was measured either by the van der Pauw method or with an Eddy current setup. Material test device fabrication [van der Pauw patterns, transmission line model (TLM) patterns, isolation patterns, and transistors] is based on the electron-beam evaporation of Ti/Al/Ni/Au for ohmic contact after etching of a part of the AlGaN barrier by inductive coupled plasma (ICP) using a Cl_2/Ar gas mixture and rapid thermal annealing in a nitrogen atmosphere at 825 °C for 30% Al content barrier devices and 850 °C for devices with an Al content above 80%. The mesa isolation was performed by ICP using Cl_2/Ar plasma. Ni/Au metal stacks were evaporated for transistor isolated gates after deposition of silicon nitride by plasma-enhanced chemical vapor deposition (PECVD). The electrical measurements were performed on-wafer using needle probes. For breakdown measurements, the samples were immersed into Fluorinert™ to avoid arching phenomena.

TABLE I. Comparison of the FWHM (in degree) of GaN (002) and GaN(302) reflection peaks for high electron mobility transistor (HEMT) structures grown on AlN substrates with different GaN channel thicknesses.

t_{AlN} (nm)	t_{GaN} (nm)	GaN (002)	GaN (302)	GaN relaxation rate (%)
300	500	0.3497	0.4424	100
250	200	…	0.561	88
250	100	0.81	0.709	72
300	50	0.8573	…	50
300	20	…	…	8
220–250	8–9	…	…	0

Structural analyses

As shown in Fig. 2, the AFM analysis of the structures clearly shows a change in the surface morphology while reducing the GaN channel thickness, from mounds induced by kinetic roughening[17] for a 500 nm GaN channel to a step flow growth morphology for 50 nm and below, with a root mean square (RMS) roughness progressively reduced from about 1 nm to less than 0.15 nm.

The FWHMs of GaN XRD rocking curves are shown in Table I. The peaks are clearly broader than the ones of AlN whose FWHMs are by far well below 0.1° and confirm the high crystal quality and low dislocation density in AlN substrates as well as in regrown AlN buffer layers. Thinning the GaN channel from 500 to 200 nm and 100 nm induces a clear broadening of the diffraction peaks, which indicates degradation in the crystal quality. This is the case for both symmetric (002) lines and asymmetric (302) ones meaning that the different types of threading dislocations [a-type, c-type, and (a + c)-type] are probably involved with bending at the origin of the peaks' widening (see later). In addition to degradation in the crystal quality, the smaller amount of the GaN material in the structure makes the intensity of diffracted peaks weaker. For this reason, the FWHMs were not studied for GaN thicknesses below 50 nm. Nevertheless, 2theta-omega scans performed around (004) reflections can provide other valuable information on the quality and strain state within HEMT structures. Figure 3 shows the 2theta-omega scans performed around the (004) reflections for HEMT structures grown with GaN thickness ranging from 500 to 9 nm. The narrow peak of AlN reflects the high crystal quality of the substrate. The GaN peak shape and position clearly evolve with the channel thickness from a narrower peak with a shoulder at low angles for thicker layers to a broader peak for the 50 nm channel. Such spectra indicate that in the first approximation, the 50 nm channel can be considered with a constant strain state and thicker layers present two regions. The first region behaves like the 50 nm layer, whereas the remaining part exhibits a noticeable change in the strain and crystal quality. Furthermore, the strain state and then the peak position of the AlGaN barrier-grown pseudomorphic on GaN follow a concomitant shift.

Table I shows the strain deduced from the calculated in-plane lattice parameter of GaN. A Poisson coefficient v = 0.45 was used to calculate the in-plane lattice parameter after extracting the c-parameter from the (004) GaN diffraction peak position. Furthermore, we added the parameters calculated from fitting XRD spectra or RSM obtained with 8, 9, and 20 nm GaN. It is clear from this table and from the corresponding plot in Fig. 4 that the GaN strain relaxation rate rapidly evolves from 0% for 8–9 nm to 8% for 20 nm, 50% for 50 nm, and almost 100% for the 500 nm GaN channel. Thus, the 20–50 nm region is the location of the most rapid change in the strain relaxation rate. To better understand this behavior, the cross-sectional STEM analysis has been performed on 50 nm and 500 nm GaN channel HEMTs. High angle annular dark field (HAADF) STEM images presented in Fig. 5 show that for both samples, a modification in the contrast and a decrease in the defect

TABLE II. Composition of active layers and comparison of the electrical properties of the DEGs for HEMT structures grown on AlN substrates.

t_{AlN} (nm)	t_{GaN} (nm)	Al content (%)	t_{AlGaN} (nm)	AlGaN relaxation rate (%)	Contactless sheet resistance (Ω/sq)	Sheet resistance (Ω/sq)	2DEG density (/cm^2)	Electron mobility (cm^2/V s)
300	500	30	19	0	420	330	1×10^{13}	1920
250	200	30	19	0	430	410	9×10^{12}	1700
250	100	30	19	0	895	840	8×10^{12}	930
300	50	30	19	0	…	1700	7.8×10^{12}	460
300	20	30	19	25	30 000	9000	2.2×10^{12}	310
250	8	30	19	19	30 000	…	…	…
250	8	82	14	0	…	21500	2×10^{12}	149
220	9	86	22	0	1300	1050	1.2×10^{13}	480
220	9	86	45	0	980	880	1.6×10^{13}	450

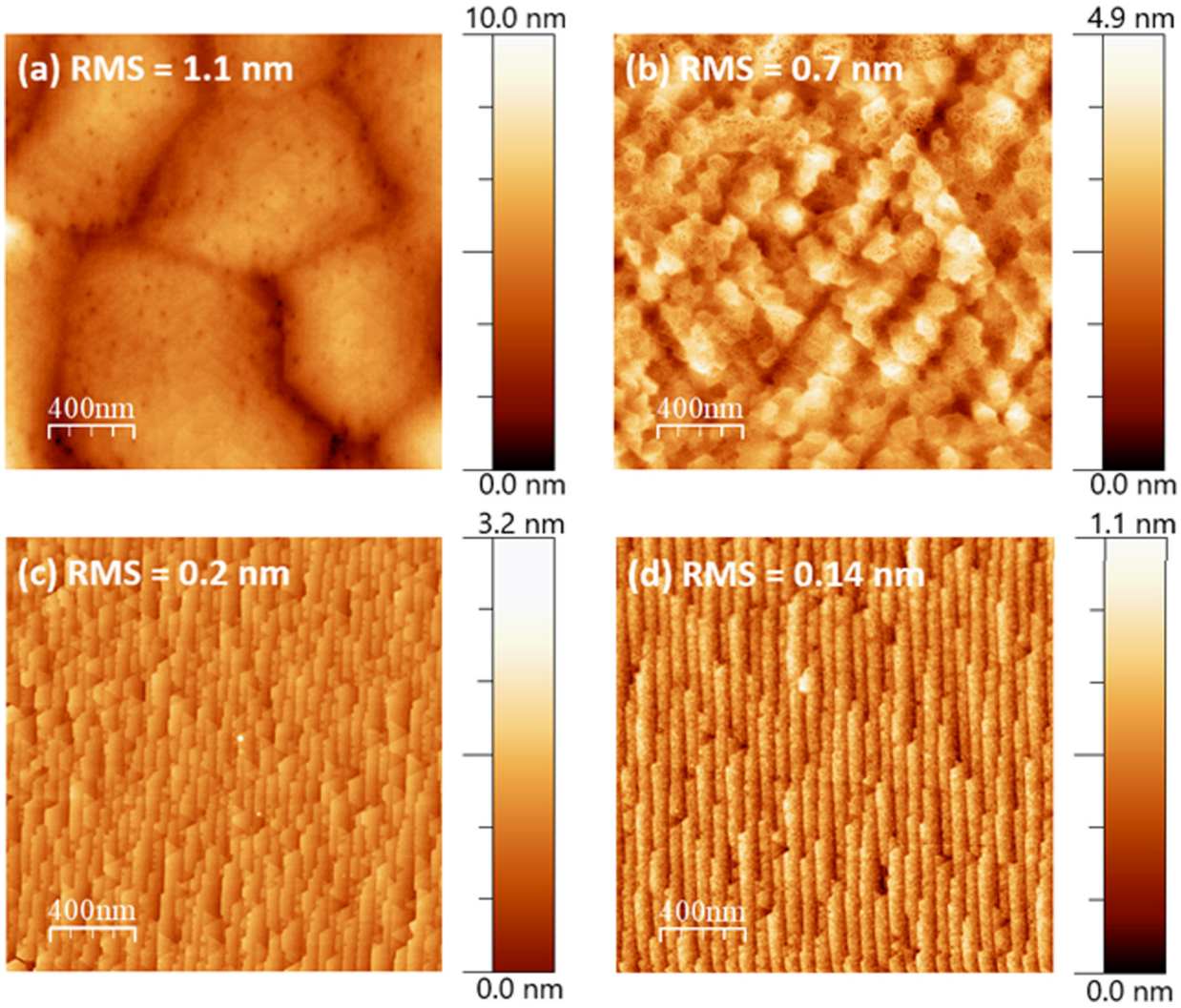

FIG. 2. AFM pictures of the surface of HEMT structures grown with (a) 500, (b) 50, (c) 20, and (d) 8 nm GaN channels.

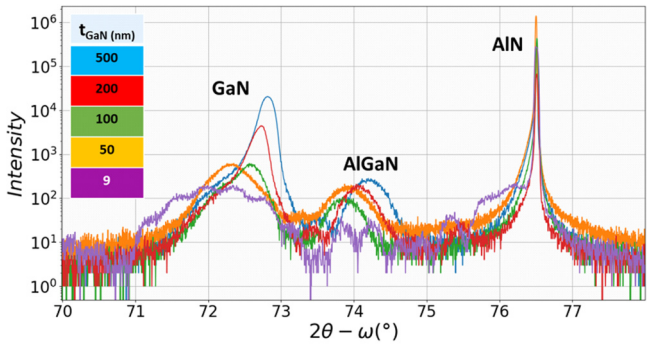

FIG. 3. XRD 2theta-omega scans performed around (004) reflections for HEMT structures grown on the AlN substrate with the GaN channel thickness ranging from 500 to 9 nm.

density occur above a 20–30 nm thick region from the GaN/AlN interface. Such observations are consistent with previous XRD analyses. Furthermore, an additional transition region with a slower change in the dislocation arrangement at about 200 nm from the GaN/AlN interface is observed in the 500 nm channel and indicated by an arrow. Such rapid and slow transition regions are regularly observed in GaN grown by NH_3-MBE on AlN nucleation layers on Si.[18] We can infer that rapid transition involves the nucleation of defects able to efficiently relax the 2.4% mismatch strain between GaN and AlN, such as misfit dislocations, and the slow transition involves a slow rate of effective climbing of threading dislocations.

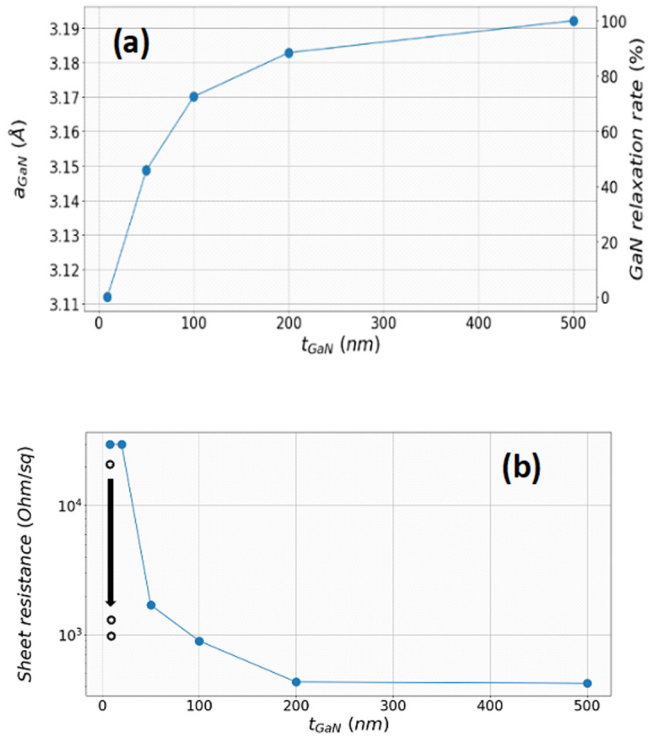

FIG. 4. (a) Evolution of strain relaxation and (b) of two-dimensional electron gas (2DEG) sheet resistance with the GaN channel thickness. The arrow emphasizes the drop of 2DEG sheet resistance in the second series of HEMT structures (open symbols).

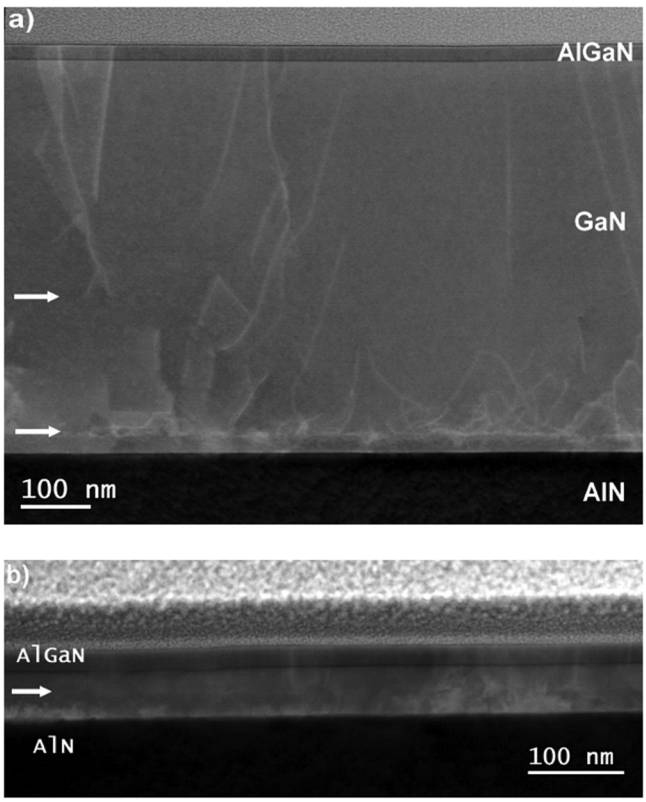

FIG. 5. Cross-sectional high angle annular dark field (HAADF)-STEM images of HEMT structures grown on the AlN substrate with GaN channel thicknesses of 500 (a) and 50 nm (b). The white arrow close to the GaN/AlN interface shows the upper limit of the first transition region in (a) and (b). The second arrow in (a) is located at about 200 nm above the first transition region and corresponds to an additional decrease in the defect density.

The present observations show that the downscaling of the channel thickness increases the residual compressive strain in GaN but at the expense of the rapprochement to a highly defective region close to GaN on the AlN interface. Nevertheless, the nucleation of defects at this interface is not likely for thicknesses below a critical value estimated around 10 nm.[19] However, maintaining a high level of compressive strain in the GaN channel reduces the in-plane lattice parameter, which results in a noticeable increase in the mismatch strain suffered by the AlGaN barrier with an Al content of 30%. Such an increase is detrimental to the pseudomorphic growth as revealed by exploitation of XRD measurements, which shows that this AlGaN barrier layer relaxed approximately 20%–25% of its

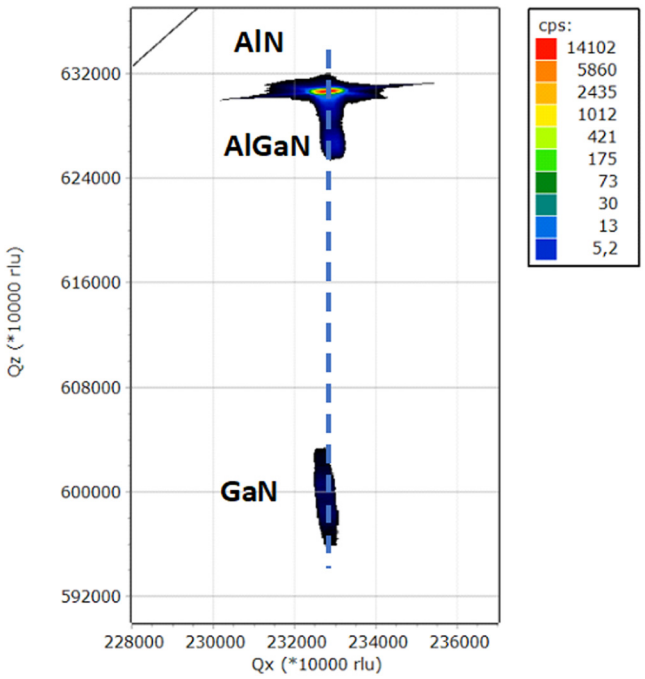

FIG. 6. XRD reciprocal space map around (105) reflections for the HEMT structure grown on the AlN substrate with the 9 nm GaN channel covered with a 22 nm thick 86% Al content AlGaN barrier.

mismatch strain with GaN. To avoid this effect, a larger Al content has to be introduced in the barrier layer in order to keep the in-plane lattice parameter close to the one of AlN.[19] In this case, the Al content in AlGaN grown on 8–9 nm GaN was increased to 82%–86%. As a result, Fig. 3 shows a very different spectrum for the 9 nm GaN channel with interference fringes attesting to the high crystal quality of the layers. Figure 6 shows the (105) RSM plot using Qx, Qy coordinates directly proportional to the reciprocal lattice parameter in the growth plane and in the growth direction, respectively. The alignment of AlN, GaN, and AlGaN barrier diffraction spots attests to in-plane lattice matching between different materials and, thus, the absence of strain relaxation in the 9 nm GaN channel nor in the 86% Al content AlGaN barrier.

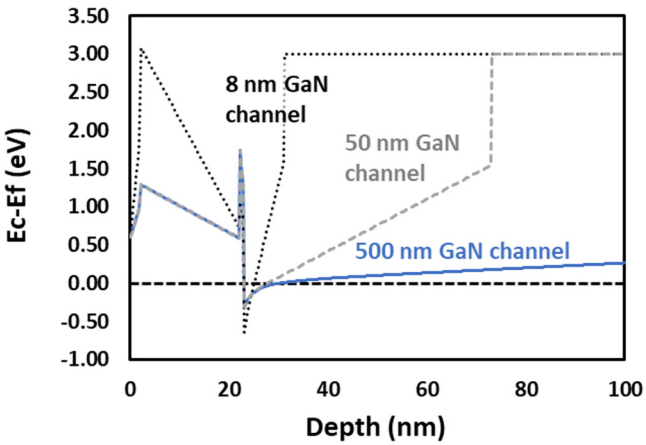

FIG. 7. Conduction band diagrams of HEMT structures with a 30% Al content AlGaN barrier on the 50 nm GaN channel (dashed line) and the 500 nm GaN channel (continuous line) and a HEMT structure with a 85% Al content AlGaN barrier on the 8 nm GaN channel (dotted line).

Electrical properties

Table II reminds the composition of the studied HEMT structures as well as the electrical properties of the 2DEGs. It is clear

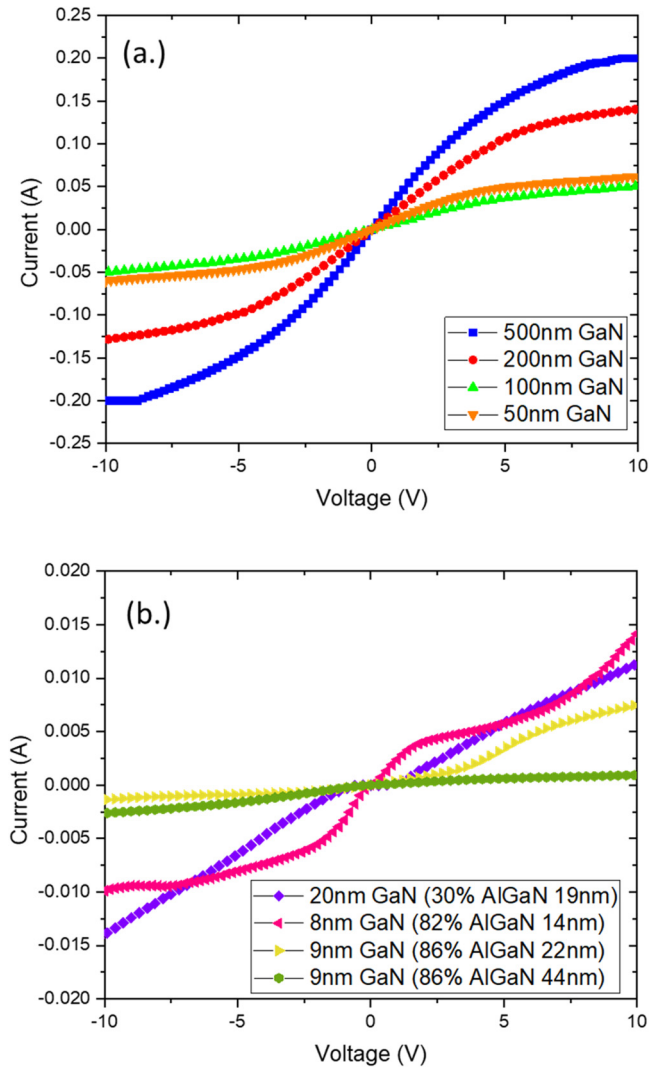

FIG. 8. I–V characteristics of 5 μm TLM spacing for various GaN channel HEMTs.

from this table and from the plot in Fig. 4 that reducing the GaN channel thickness down to 50 nm results in a regular increase in the sheet resistance from 330 to 1700 Ω/sq. The reduction in the carrier density is partly due to the upraising of the conduction band linked to the negative polarization charge present at the GaN/AlN interface as shown in Fig. 7 and the reduction in the polarization discontinuity due to the strained GaN. This reduction in the carrier density accounts less for the increase in the resistance than significant degradation in electron mobility related to the lower crystal quality. Indeed, the thinning of the GaN channel from 500 to 50 nm decreases the 2DEG density from 1×10^{13} to $7.8 \times 10^{12}/cm^2$, whereas the mobility drops from 1920 to 460 cm^2/V s. Hg-CV profiles of these heterostructures confirm this trend with no change of capacitance at Vg = 0 V attesting no variation of the location in the 2DEG but a shift of the pinch-off voltage toward positive values confirming the reduction in the 2DEG density (supplementary material **S1**). The electron mobility continues to degrade with a further reduction in GaN channel thickness while keeping a 30% Al content AlGaN barrier, which dramatically impacts the sheet resistance that reaches 30 kΩ/sq. for the 8 nm GaN channel. As previously evocated, the sub-10 nm GaN channel is sufficiently thin to inhibit strain relaxation, but at the expense of an increase in the mismatch between the 30% Al content barrier and the underlying layers possessing the in-plane lattice parameter of AlN. Using the same formalism as in Ref. 19, one can estimate that such a barrier presents a lattice mismatch f = 1.7% and the critical thickness $t_{cr} = b_e/2f$, where $b_e = 0.31$ nm is the Burgers vector, is below 10 nm. As a result, it is not surprising that the 19 nm thick AlGaN barrier with 30% Al content suffers strain relaxation with highly degraded 2DEG carrier density and transport properties for 8 and 20 nm width channel HEMTs. On the other hand, the sheet resistance is only slightly reduced from 30 to about 20 kΩ/sq. while increasing to 82% of the Al content in the barrier grown on the 8 nm GaN channel. A possible explanation for a 2DEG carrier density limited to $2 \times 10^{12}/cm^2$ is the 14 nm thickness of the barrier, which is not sufficient to induce an efficient transfer of electrons from surface donor states to

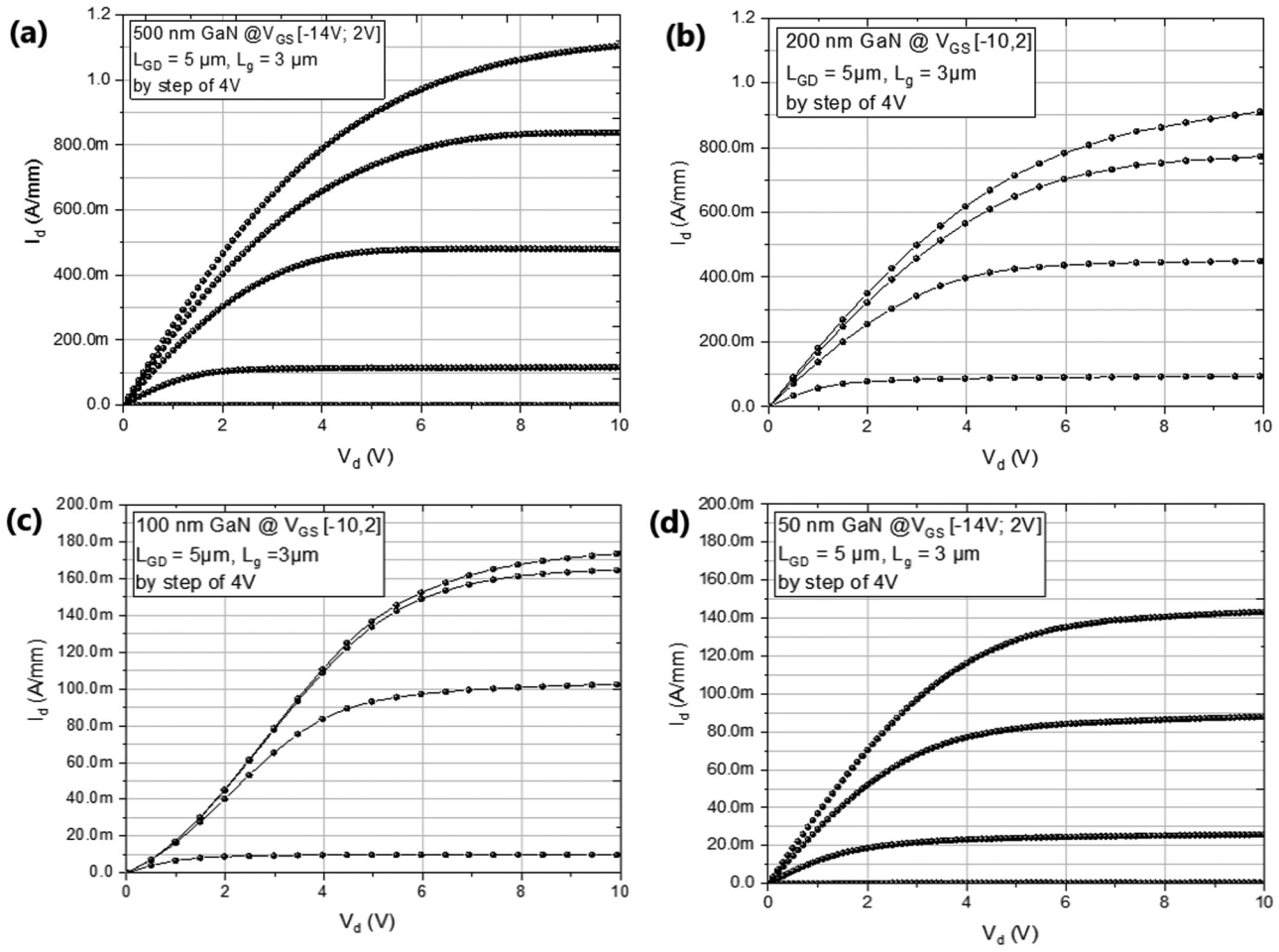

FIG. 9. DC output characteristics Id–Vd of 3 μm gate transistors fabricated on HEMT structures with (a) 500, (b) 200 , (c) 100, and (d) 50 nm GaN channels.

the GaN channel.[20] The HEMT structures grown with 22 and 45 nm thick barriers with a similar Al content of 86% on a 9 nm GaN channel confirm this hypothesis with 2DEG densities enhanced to 1.2×10^{13} and $1.6 \times 10^{13}/cm^2$, respectively, resulting in sheet resistances of 1050 and 880 Ω/sq. Figure 7 also illustrates the benefit of introducing such kind of barrier as the conduction band in GaN is well below the Fermi level at the interface where the 2DEG is generated. Examples of conduction band diagrams and carrier profiles of structures presented in Fig. 7 are shown in supplementary material **S2**. On the other hand, the electron mobility in these last structures is around 450 cm^2/V s, which is similar to the one previously extracted from the 50 nm GaN channel HEMT. Compared with the 136–195 cm^2/V s mobility obtained previously on sapphire[14] with a similar 2DEG carrier density, this attests to the quality of the layers grown perfectly strained on the AlN substrate.

Finally, the current–voltage characteristics of transistors processed on these HEMT structures have been studied. The transfer length method (TLM) I–V characteristics for 5 μm contact spacing is shown in Fig. 8 for various GaN channel HEMTs. Figure 8(a) shows the ohmic behavior of 500–50 nm GaN channel devices. It clearly portrays the degradation of ohmic contact with channel thickness downscaling. The effect of the Al-rich AlGaN barrier and its thickness on achieving ohmic contact to the thin GaN channel is shown in Fig. 8(b). Considering Al-rich AlGaN barrier, the contact to 2DEG becomes difficult, even with partial barrier etching technique and alternative way such as n + GaN regrowth technique needs to be tested. The DC output characteristics Id–Vd of transistors fabricated on HEMT structures with 500, 200, 100, and 50 nm GaN channels are shown in Fig. 9. The gate length of these transistors is 3 μm, while the drain to gate distance is 5 μm. At $V_g = 2$ V and $V_d = 10$ V, a maximum drain current density of 1.1 A/mm is obtained for the 500 nm GaN channel device, whereas it drops to 140 mA/mm for the 50 nm GaN channel device. This is consistent with the increase from 0.5 to 3.4 mΩ cm^2 of the static on-resistance of these devices. Although the transistors are fully functional, the difficulty in achieving low resistance ohmic contacts (<1 Ω mm) with a GaN channel width of 100 nm or less can be noticed. The on-state drain current density limitation is observed in the 100 nm GaN channel device, which is due to the poor ohmic contact with 2DEG as compared to the 50 nm GaN channel device.

On the other hand, low leakage current (1 μA/mm or less) is obtained at pinch-off and on-state currents are consistent with the sheet resistance of the 2DEGs as shown by Id–Vg transfer characteristics in Fig. 10. As previously noticed with Hg-CV measurements performed on as-grown heterostructures, GaN channel thinning while keeping the barrier thickness constant induces a threshold voltage shift toward positive values consistently with the reduction in the 2DEG density. The large negative threshold voltage is due to the 30 nm thick SiN gate insulator deposited by PECVD at 340 °C. The use of an MIS type structure is to suppress the gate leakage when the device is operating at high voltage. A Schottky gate contact definitely induces gate leakage under a high electric field, which is mitigated by the gate insulator in order to properly evaluate the material properties. The present PECVD deposited SiN has a breakdown field of 9 MV/cm as extracted through the vertical breakdown measurements of various film thicknesses. As shown in Fig. 10(c), drain current hysteresis is

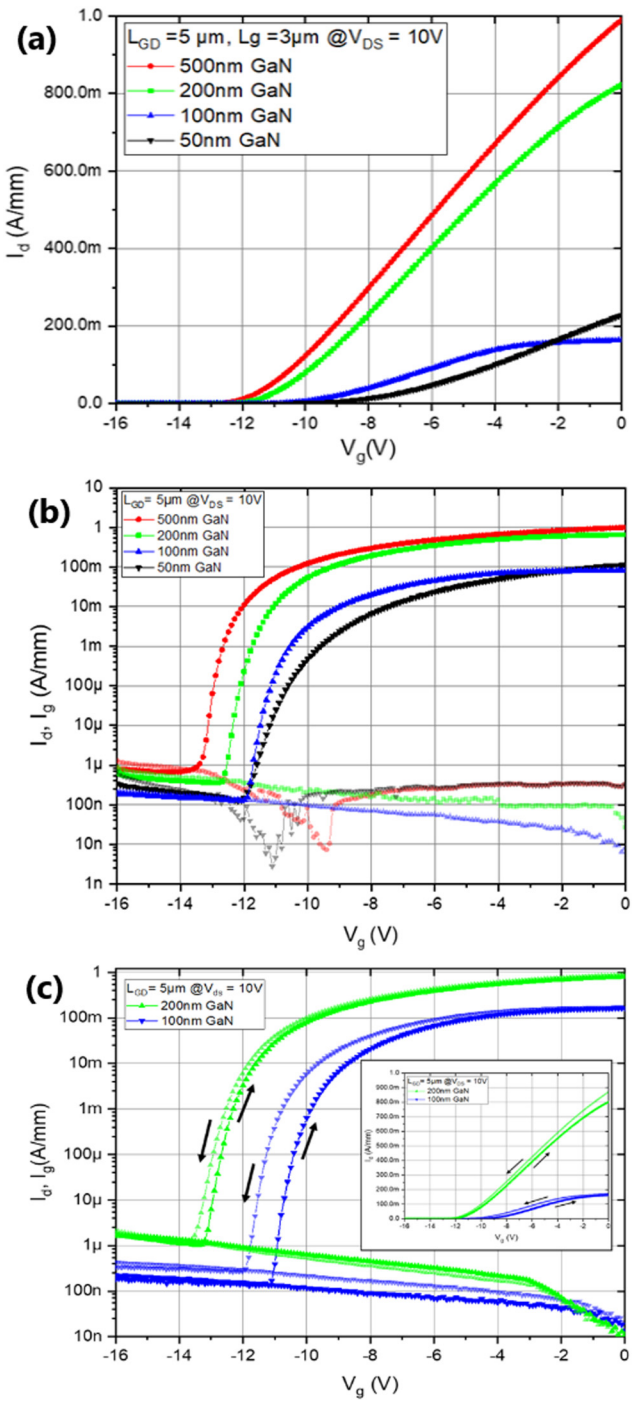

FIG. 10. (a) Id–Vg characteristics of 3 μm gate transistors on AlGaN/GaN HEMT structures on AlN with GaN channel thicknesses of 50, 100, 200, and 500 nm. (b) Semi-log plots of Id–Vg and Ig–Vg characteristics of same devices. (c) Semi-log plots of Id–Vg and I_g–V_g characteristics of 100 and 200 nm GaN channel transistors with V_g sweeping from 0 to −16 V and then from −16 to 0 V (the inset shows the linear plots of I_d–V_g).

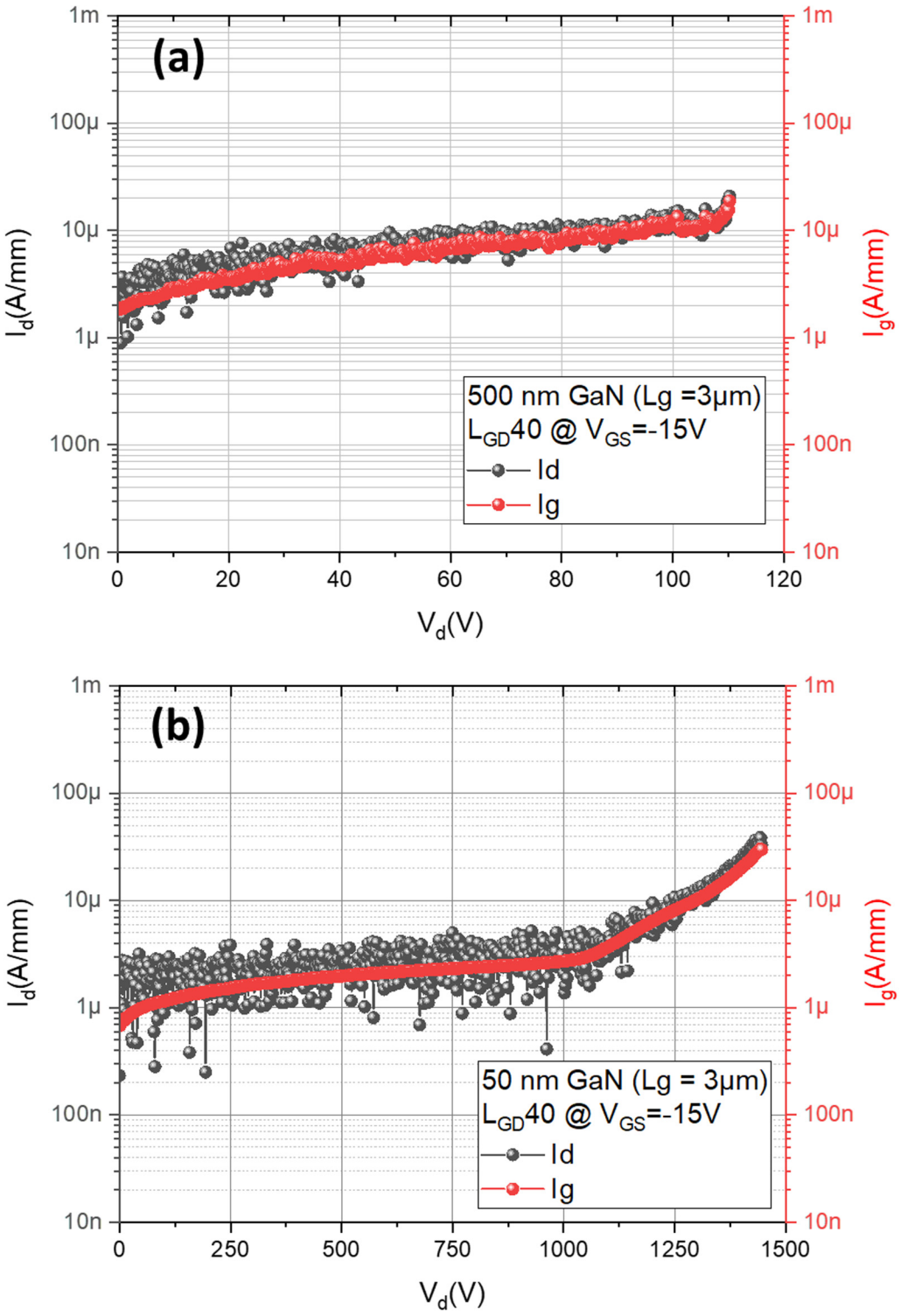

FIG. 11. Off-state leakage current characteristics of transistors on AlGaN/GaN HEMT structures on AlN with GaN channel thicknesses of (a) 500 and (b) 50 nm. The gate length is 3 μm, and the gate to drain distance is 40 μm.

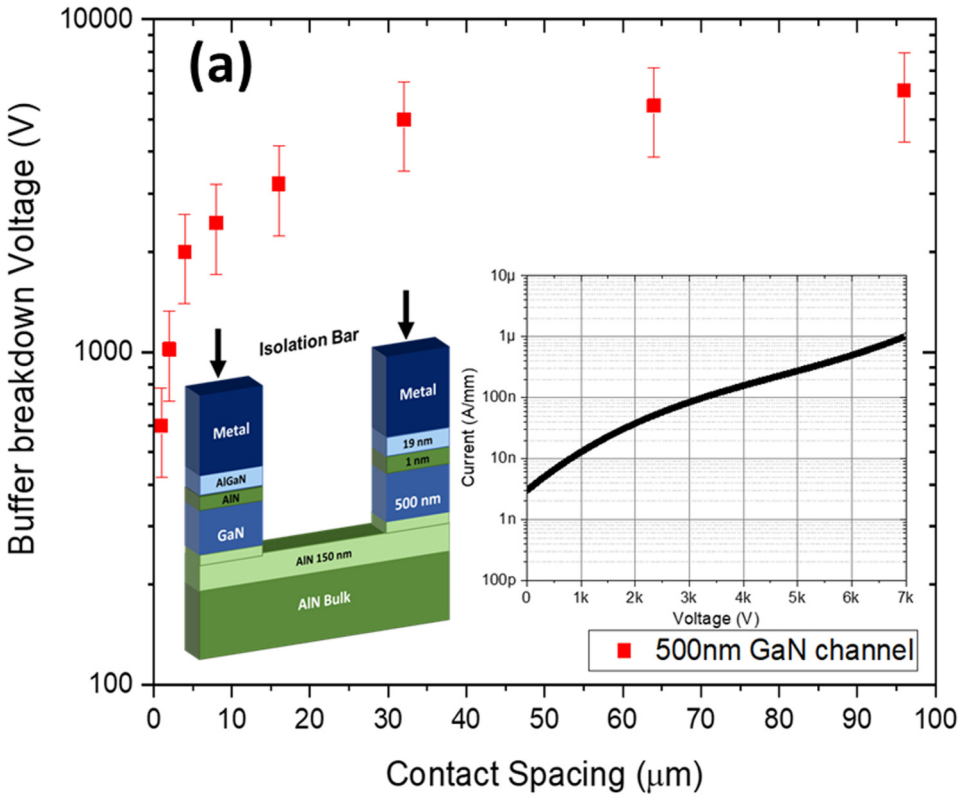

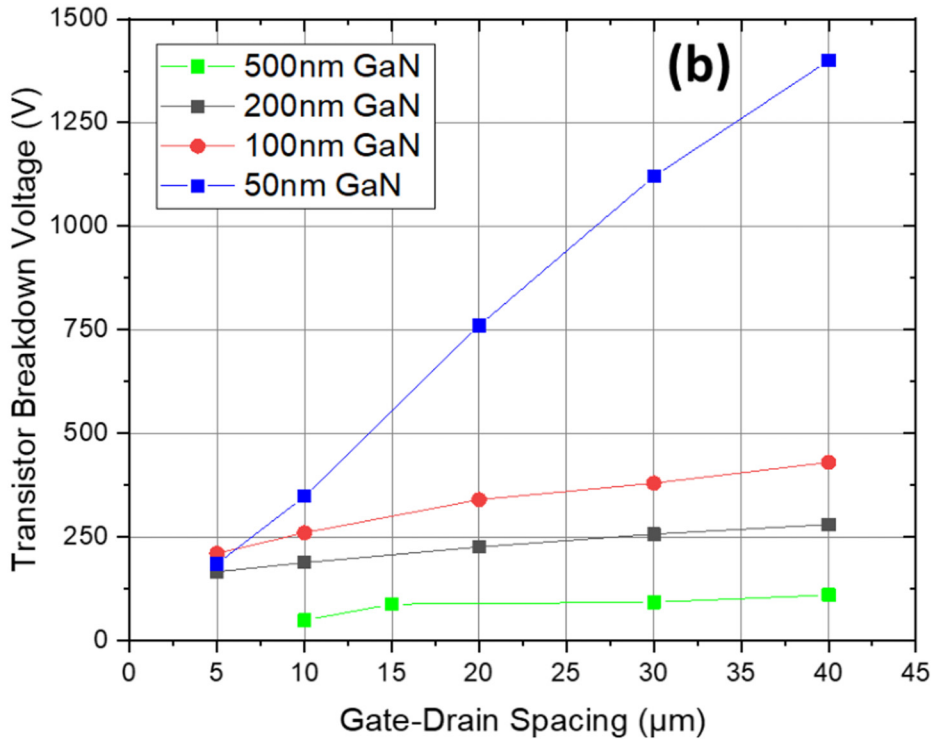

FIG. 12. (a) Lateral buffer breakdown vs contact spacing. (b) Three-terminal transistor breakdown voltage of AlGaN/GaN HEMT structures on AlN vs gate to drain spacing.

noticed while sweeping the gate bias V_g backward and then upward between 0 and −16 V. The positive shift in the threshold voltage indicates a more important trapping effect of electrons in the 100 nm GaN channel transistor compared to the 200 nm GaN channel. This slightly reduces the gate leakage current Ig, which may be due to the proximity of the 2DEG with the defective region identified at the GaN/AlN interface shown in Fig. 5.

The three-terminal breakdown behavior of transistors fabricated with a gate to drain distance L_{GD} of 40 μm on HEMT structures with 50 and 500 nm thick GaN channels is shown in Fig. 11. Interestingly, the 50 nm channel transistor delivered about 10 times higher breakdown voltage (BV) (defined at 100 μA/mm) than the 500 nm thick channel one and reached more than 1400 V with static $R_{on} = 32\ m\Omega\ cm^2$. Figure 12(a) shows the lateral buffer BV between $100 \times 100\ \mu$m isolated ohmic contacts with various distances. The inset shows the leakage current below 1 μA/mm for 96 μm contact spacing up to 7000 V, revealing no parasitic leakage through mesa sidewalls. With a BV above 3 kV for 15 μm contact spacing, the AlN buffer seems likely to permit the fabrication of transistors with breakdown scaling with a gate–drain distance, as shown in Ref. 21. The present results also show that none of the two structures suffers electron injection or its consequences into the AlN substrate. This behavior is different from the trend previously observed for the structures we studied with 8 and 240 nm GaN channels on sapphire,[8] in which a degraded lateral buffer breakdown voltage was noticed for the thicker channel HEMT. To explain this difference, we suppose that the less efficient confinement of electrons in the wider GaN channel[22] enabled their injection toward the AlN buffer that was not free of defects because grown lattice mismatched on sapphire.[14] On the other hand, the presence of much fewer defects in the buffer and the AlN substrate makes the previous explanation less likely for the three-terminal breakdown, so we can suppose that in this case, the weaker confinement in the wider channel enabled electrons from the 2DEG to interact with the defects evidenced at the GaN/AlN interface shown in Fig. 5. Further reduction in the channel width down to 8 nm shows the same trend for the lateral buffer breakdown, which may confirm our hypothesis. However, the different isolation processes used in Ref. 8 may also account for different behaviors of buffer layers and a more detailed electrical analysis, such as the one developed in Ref. 23, will be necessary to confirm the root causes of observed degradations of the blocking strength of the transistors. Figure 12(b) shows the three-terminal breakdown voltage of transistors fabricated with gate to drain distances varying between 5 and 40 μm. The monotonous increase in the breakdown voltage attests the homogeneity of the breakdown electric field. Furthermore, the plot confirms the noticeable increase in the breakdown voltage when the GaN channel thickness is reduced down to 50 nm. Technical difficulties led to a larger leakage in the transistors fabricated on the thinner channel structures (8–20 nm GaN channels) and resulted in a lower three-terminal breakdown voltage. Nevertheless, the electron confinement in such structures seems sufficiently performant to prevent devices with GD = 40 μm from hard breakdown for drain voltages up to 1.4 kV. Thus, despite the degradation of the leakage current we attribute to our non-mature device process, these results are encouraging for the development of a perfectly strained HEMT structure for high voltage applications.

CONCLUSIONS

In the present work, two series of AlGaN/GaN/AlN HEMT structures have been grown on bulk AlN substrates by molecular beam epitaxy to study the effect of GaN channel width downscaling. In the first series of HEMT structures grown with a moderate aluminum content of 30% in the AlGaN barrier, the channel thinning produces a reduction in the GaN strain relaxation rate but at the expense of a rapprochement with the crystal quality degraded region whose thickness is estimated around 20–30 nm and located close to the GaN/AlN interface. A first consequence is a degradation of the electron mobility in the 2DEG and a noticeable increase in the sheet resistance. On the other hand, sub-10 nm GaN channels have been grown perfectly strained and defect free, but they necessitate a high aluminum content AlGaN barrier to induce 2DEGs with high sheet carrier densities as studied in the second series. In this case, similar electron mobility is obtained as in a partly relaxed 50 nm GaN channel but with a noticeably larger carrier density, which is an advantage for high power applications. Finally, the buffer lateral breakdown and the three-terminal breakdown behavior of transistors have been studied. Contrary to previously studied HEMT structures on the sapphire substrate, all the present structures follow the same trend for the dependence of buffer lateral breakdown with an isolated contact distance, independent of the channel width, indicating that none of the latter suffers electron injection or its consequences into the AlN substrate, which highlights the importance of the AlN crystal quality on the buffer breakdown. However, in spite of the better crystal quality of the 500 nm GaN channel receiving the 2DEG, a reduced three-terminal breakdown voltage of around 100 V has been measured. We attribute this behavior to a lack of confinement of electrons able to interact with defects located close to the bottom GaN/AlN interface. On the contrary, the electric field distribution in thinner GaN channel HEMT structures impinges this phenomenon, so we can consider that better carrier confinement operates in these structures. As a consequence, two kinds of optimized HEMT structures emerge from this study. First, a trade-off between the crystal quality and 2DEG confinement emerges with a partly strained relaxed 50 nm GaN channel transistor able to sustain 1400 V with a 2DEG sheet resistance of 1700 Ω/sq. while keeping a moderate aluminum content in the AlGaN barrier. Second, perfectly strained 8–9 nm GaN channel HEMT structures have been achieved with an aluminum-rich AlGaN barrier delivering a 2DEG sheet resistance below 900 Ω/sq. with transistors showing hard breakdown voltages in the same range in spite of a noticeable leakage current we attribute to a lack of maturity of the device process. Even if further optimizations of such new HEMTs are needed, the latter may constitute the next building block for high power switching transistors.

SUPPLEMENTARY MATERIAL

See the supplementary material, **S1** for the Hg-CV measurements of HEMTs and **S2** for simulated band diagrams and electron density profiles.

ACKNOWLEDGMENTS

This work was supported by the French RENATECH Network, the project BREAKUP (French National Research Agency Grant No.

ANR-17-CE05–0013), and the project HBV of the "Investissements d'Avenir" Program GaNeX (Grant No. ANR-11-LABX-0014).

AUTHOR DECLARATIONS

Conflict of Interest

The authors have no conflicts to disclose.

Author Contributions

R. Elwaradi: Formal analysis (equal); Investigation (equal); Resources (equal); Writing – original draft (equal); Writing – review & editing (equal). **J. Mehta:** Formal analysis (equal); Investigation (equal); Resources (equal); Writing – original draft (equal); Writing – review & editing (equal). **T. H. Ngo:** Formal analysis (equal); Investigation (equal); Writing – original draft (equal); Writing – review & editing (equal). **M. Nemoz:** Formal analysis (equal); Investigation (equal); Writing – original draft (supporting). **C. Bougerol:** Formal analysis (equal); Investigation (equal); Writing – original draft (equal). **F. Medjdoub:** Formal analysis (equal); Funding acquisition (equal); Investigation (equal); Project administration (equal); Writing – original draft (equal); Writing – review & editing (equal). **Y. Cordier:** Conceptualization (lead); Data curation (equal); Formal analysis (equal); Funding acquisition (equal); Investigation (equal); Project administration (equal); Resources (lead); Supervision (lead); Writing – original draft (equal); Writing – review & editing (equal).

DATA AVAILABILITY

The data that support the findings of this study are available from the corresponding author upon reasonable request.

REFERENCES

[1]O. Ambacher, B. Foutz, J. Smart, J. R. Shealy, N. G. Weimann, K. Chu, M. Murphy, A. J. Sierakowski, W. J. Schaff, and L. F. Eastman, J. Appl. Phys. **87**, 334–344 (2000).
[2]R. J. Kaplar, A. A. Allerman, A. M. Armstrong, M. H. Crawford, J. R. Dickerson, A. J. Fischer, A. G. Baca, and E. A. Douglas, "Review—Ultra-wide-bandgap AlGaN power electronic devices," ECS J. Solid State Sci. Technol. **6**, Q3061–Q3066 (2017).
[3]T. J. Anderson, J. K. Hite, and F. Ren, "Ultra-wide bandgap materials and device," ECS J. Solid State Sci. Technol. **6**, Y1 (2017).
[4]J. Y. Tsao, S. Chowdhury, M. A. Hollis, D. Jena, N. M. Johnson, K. A. Jones, R. J. Kaplar, S. Rajan, C. G. Van De Walle, E. Bellotti *et al.*, "Ultrawide-bandgap semiconductors: Research opportunities and challenges," Adv. Electron. Mater. **4**, 1600501 (2018).
[5]S. Kume, I. Yamada, K. Watari, I. Harada, and K. Mitsuishi, "High-thermal-conductivity AlN filler for polymer/ceramics composites," J. Am. Ceram. Soc. **92**, S153–S156 (2009).
[6]J. R. Shealy, V. Kaper, V. Tilak, T. Prunty, J. A. Smart, B. Green, and L. F. Eastman, J. Phys.: Condens. Matter **14**, 3499–3509 (2002).
[7]N. Yafune, S. Hashimoto, K. Akita, Y. Yamamoto, H. Tokuda, and M. Kuzuhara, Electron. Lett. **50**, 211–212 (2014).
[8]I. Abid, R. Kabouche, C. Bougerol, J. Pernot, C. Masante, R. Comyn, Y. Cordier, and F. Medjdoub, Micromachines **10**, 690 (2019).
[9]T. Nanjo, M. Takeuchi, M. Suita, T. Oishi, Y. Abe, Y. Tokuda, and Y. Aoyagi, Appl. Phys. Lett. **92**, 263502 (2008).
[10]Z. X. Wang, L. Du, J. W. Liu, Y. Wang, Y. Jiang, S. W. Ji, S. W. Dong, W. W. Chen, X. H. Tan, J. L. Li *et al.*, Chin. Phys. B **29**, 027301 (2020).
[11]A. Raman, S. Dasgupta, S. Rajan, J. S. Speck, and U. K. Mishra, Jpn. J. Appl. Phys. **47**, 3359–3361 (2008).
[12]Z. Li, L. Du, J. Lou, Y. Jiang, K. Wang, W. Wen, Z. Wang, S. Zhao, J. Zhang, and Y. Hao, Phys. Status Solidi A **217**, 1900793 (2020).
[13]I. Abid, J. Mehta, Y. Cordier, J. Derluyn, S. Degroote, H. Miyake, and F. Medjdoub, Electronics **10**, 635 (2021).
[14]J. Bassaler, R. Comyn, C. Bougerol, Y. Cordier, F. Medjdoub, and P. Ferrandis, J. Appl. Phys. **131**(12), 124501 (2022).
[15]Y. Cordier, F. Pruvost, F. Semond, J. Massies, M. Leroux, P. Lorenzini, and C. Chaix, Phys. Status Solidi C **3**, 2325–2328 (2006).
[16]See https://www.hexatechinc.com/documents/HexaTech-AlN-10-Datasheet-PD-AlN-10-R004.pdf for information about AlN bulk substrates.
[17]S. Vézian, F. Natali, F. Semond, and J. Massies, Phys. Rev. B **69**, 125329 (2004).
[18]N. Baron, Y. Cordier, S. Chenot, P. Vennéguès, O. Tottereau, M. Leroux, F. Semond, and J. Massies, J. Appl. Phys. **105**, 033701 (2009).
[19]R. Chaudhuri, A. Hickman, J. Singhal, J. Casamento, H. Grace Xing, and D. Jena, Phys. Status Solidi A **219**, 2100452 (2022).
[20]J. P. Ibbetson, P. T. Fini, K. D. Ness, S. P. DenBaars, J. S. Speck, and U. K. Mishra, Appl. Phys. Lett. **77**, 250–252 (2000).
[21]O. Hilt, F. Brunner, E. B. Treidel, M. Wolf, and J. Würfl, in *2021 Device Research Conference (DRC)*, Santa Barbara, CA (IEEE, 2021), pp. 1–2.
[22]M. J. Uren, K. J. Nash, R. S. Balmer, T. Martin, E. Morvan, N. Caillas, S. L. Delage, D. Ducatteau, B. Grimbert, and J. C. De Jaeger, IEEE Trans. Electron Devices **53**(2), 395–398 (2006).
[23]S. R. Bahl and J. A. del Alamo, IEEE Trans. Electron Devices **40**(8), 1558–1560 (1993).